A phosphorus-containing tertiary amine hardener enabled flame retardant, heat resistant and mechanically strong yet tough epoxy resins

Qingshan Yang [a], Jun Wang [a,b], Xi Chen [b], Shuang Yang [b,*], Siqi Huo [c,*], Qiufei Chen [d], Pengzong Guo [d], Xiao Wang [d], Fu Liu [d], Wei Chen [e], Pingan Song [c,f], Hao Wang [c]

[a] School of Materials Science and Engineering, Wuhan University of Technology, Wuhan 430070, China
[b] School of Mechanical and Electronic Engineering, Wuhan University of Technology, Wuhan 430070, China
[c] Centre for Future Materials, University of Southern Queensland, Springfield 4300, Australia
[d] Zhongfu Shenying Carbon Fiber Co., Ltd, Lianyungang, China
[e] School of Civil Engineering, Architecture and Environment, Hubei University of Technology, Wuhan 430068, China
[f] School of Agriculture and Environmental Science, University of Southern Queensland, Springfield 4300, Australia

ARTICLE INFO

ABSTRACT

Although current phosphorus (P)-based hardeners endowed epoxy resins (EPs) with intrinsic flame retardancy, their addition usually reduced thermal and mechanical properties. In this work, a novel phosphorus-containing tertiary amine hardener (DCM) was synthesized using diphenylphosphinic chloride and 2,4,6-tris(dimethylaminomethyl)phenol (DMP-30), and applied to fabricate high-performance EP/DCM. Introducing P-containing group reduced the reactivity of tertiary amine of DCM, but EP/DCM gelled at 100 °C within 11.3 min, showing modest-temperature curing character. EP/DCM exhibited higher glass-transition temperature (T_g) and char yield than virgin EP/DMP-30. Moreover, EP/DCM featured superior mechanical properties, of which the tensile strength, elongation at break and impact strength increased by 61.2%, 72.0% and 198.5%, respectively, relative to those of EP/DMP-30. DCM endowed EP thermosets with remarkable flame retardancy and smoke suppression. The limiting oxygen index (LOI) and UL-94 rating of EP/DCM reached 35.7% and V-0, respectively, with 36.2% and 22.6% reductions in peak heat release rate (PHRR) and peak smoke production rate (PSPR) compared with those of EP/DMP-30. This work pioneers an innovative strategy for creating high-performance EPs with satisfactory heat resistance, fire safety, and mechanical properties by curing with P-containing tertiary amine hardeners.

1. Introduction

Epoxy resin (EP), as one kind of ubiquitous thermosetting polymer, is widely applied in various industries owing to its excellent electrical insulation, mechanical properties, adhesive strength, processability, and dimensional stability [1–3]. However, EP is intrinsically combustible, and will release plenty of heat and smoke during combustion, which may seriously threaten human lives and properties. Hence, the application of EP in the fields with high requirements for flame-retardant performances is severely restricted [4,5]. To expand the application scope of EP in modern industries, many efforts have been devoted to addressing its flammability issue in recent years [6–8].

Introducing flame retardants is effective in enhancing the flame retardancy of polymeric materials [9,10]. Although halogen-based

flame retardants exhibit outstanding flame-retardant functions, most of them are gradually eliminated from the market due to their severe environmental pollution and massive toxic gas emissions during combustion [11–13]. P-based flame retardants have attracted increasing attention from researchers and engineers because of their high efficiency and multiple flame-retardant functions [14,15]. To endow EP with inherent flame retardancy, various phosphorus-containing curing agents have been developed recently, including phosphorus-containing anhydrides [16–18], amines [19–21], and imidazoles [22–24]. For example, Huang et al. [25] synthesized two P-derived anhydride curing agents (Car-DCP-MAH and Car-DPC-MAH) to improve the fire safety of EP. Their results indicated that the as-prepared EP/Car-DCP-MAH and EP/Car-DPC-MAH showed improved flame retardancy, of which the LOI values reached 29.0% and 28.0%, respectively. Moreover, both EPs

---

* Corresponding authors.

achieved a UL-94 V-0 rating. Nevertheless, the incorporation of Car-DCP-MAH and Car-DPC-MAH resulted in significant decreases in the tensile strength and Young's modulus of EPs. Ai *et al.* [21] reported a phosphorus-containing triazolyl amine (P-ATA) for fabricating inherently flame-retardant EPs. The P-ATA-containing EP showed enhanced flame-retardant performances, which achieved a LOI of 33.1% with a 55.7% reduction in PHRR compared with virgin EP. However, the introduction of P-ATA caused EP to produce more smoke during combustion and reduced the T_g. Recently, our team [26–28] developed some P-containing imidazole curing agents to prepare flame-retardant one-component EP systems. Our results indicated that the obtained EPs exhibited outstanding flame retardancy, as evidenced by the LOI values of 31.3–35.3% and UL-94 V-0 rating. However, these flame-retardant EP systems also suffered from unsatisfactory thermal and mechanical properties. These works had clearly demonstrated that the P-containing curing agents can effectively solve the inherent flammability problem of EPs, but their negative impacts on thermal and mechanical performances cannot be ignored.

DMP-30 is able to initiate the anionic polymerization of epoxy resin due to its tertiary amine-rich structure, which is frequently applied as an accelerator to increase the curing rate and reduce the curing temperature of EP/anhydride system [29–31]. However, the tertiary amine group in DMP-30 can cure epoxy resin rapidly once EP and DMP-30 are mixed, resulting in a short operational time of EP/DMP-30 system. More importantly, the EP/DMP-30 system releases abundant heat during the curing reaction, which causes high residual thermal stress of the cured product, thus deteriorating the thermal and mechanical properties. Although the EP/DMP-30 system can be cured at relatively low temperatures, it suffers from poor processability, heat resistance and mechanical properties. Similar to other EP systems, the flammability issue of EP/DMP-30 also needs to be addressed urgently.

Herein, a phosphorus-containing tertiary amine curing agent (DCM) with multiple functions was synthesized by the reaction of DPPC and DMP-30, and applied to develop high-performance, fire-safe epoxy resins. The chemical structure of DCM was confirmed by different measurements, and its influences on the curing/rheological behaviors, thermal properties, mechanical performances, flame retardancy and smoke suppression of EP were evaluated systematically. Furthermore, the toughening and flame-retardant mechanisms of DCM were investigated in detail. This work not only expands the type of phosphorus-containing curing agent, but also creates a class of advanced fire-safe EPs which can be cured at modest temperatures.

2. Experimental section

2.1. Materials

Diphenylphosphinic chloride (DPPC) was purchased from Heowns Biochemical Technology Co., Ltd (Tianjin, China). 2,4,6-Tris(dimethylaminomethyl)phenol (DMP-30), triethylamine (TEA), and tetrahydrofuran (THF) were provided by Aladdin Reagents Co., Ltd (Shanghai, China). Bisphenol A type epoxy resin (DGEBA) with an epoxide equivalent weight of about 188 g/eq was obtained from Yueyang Baling Huaxing Petrochemical Co., Ltd (Hunan, China).

2.2. Synthesis of DCM

DCM was synthesized *via* the elimination reaction between DMP-30 and DPPC, with the synthesis route illustrated in Fig. 1a. Firstly, DMP-30 (13.27 g), TEA (5.06 g) and THF (50 mL) were transferred into a three-necked flask and stirred at room temperature for 10 min to form a homogeneous solution. Then, DPPC (11.83 g) dissolved in THF (50 mL) was slowly dripped into the flask. After that, the mixture was heated up to 60 °C, and stirred continuously for 5 h. The triethylamine hydrochloride and THF were removed by filtration and distillation. Finally, the yellow liquid product (DCM) was obtained, and dried under vacuum at 90 °C for 5 h (Yield: 93%).

2.3. Preparation of EP thermosets

The formulas of EP/DMP-30 and EP/DCM samples are listed in Table 1, and the preparation is as follows. The curing agent (DMP-30 or DCM) was introduced into DGEBA and stirred continuously at room temperature until becoming transparent. Then, the obtained solution
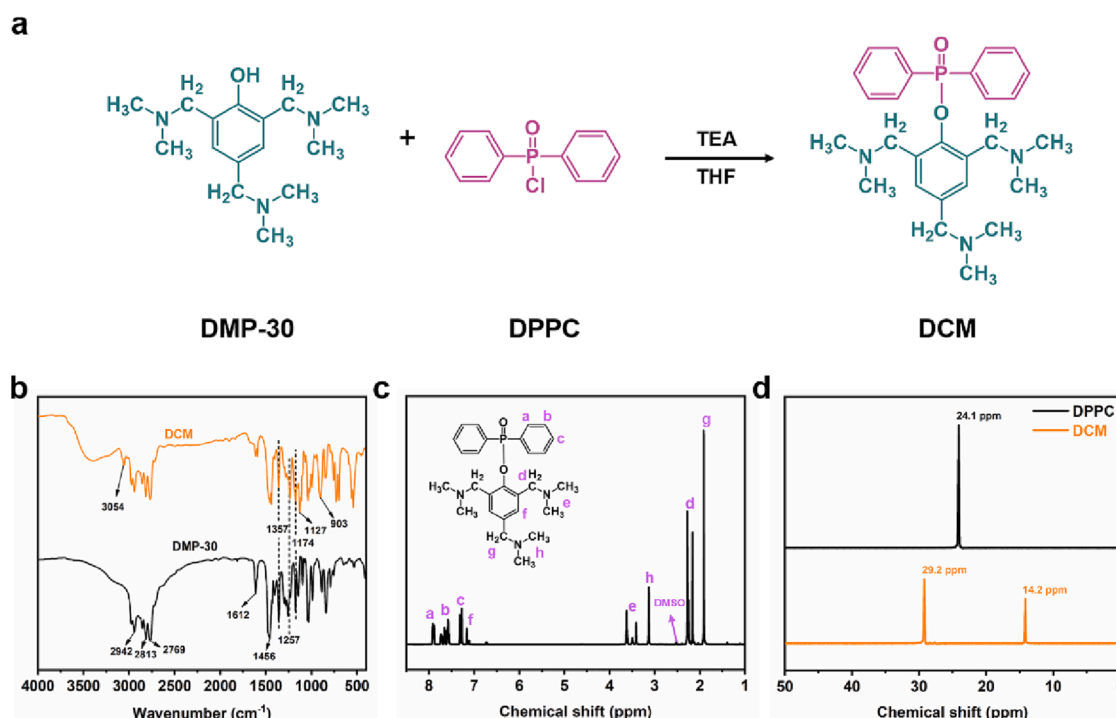

Fig. 1. (a) Synthesis route of DCM; (b) FTIR spectra of DMP-30 and DCM; (c) ^1H NMR spectrum of DCM; and (d) ^{31}P NMR spectra of DPPC and DCM.

Table 1
Formulas of EP thermosets.

Sample code	DGEBA (g)	DMP-30 (g)	DCM (g)	P content (wt%)
EP/DMP-30	100	13	/	/
EP/DCM-0.75	100	/	12.7	0.75
EP/DCM-1	100	/	17.7	1.0
EP/DCM-1.25	100	/	23.1	1.25
EP/DCM-1.5	100	/	29.1	1.5

was defoamed for 3 min, and a small amount of it was collected for studying the curing and rheological behaviors. Finally, the solution was introduced into a mold that was pre-heated at 50 °C, and cured at 90 °C for 1 h, 130 °C for 2 h, and 160 °C for 3 h.

2.4. Measurements

Fourier transform infrared (FTIR) spectra were recorded on a Nicolet 6700 infrared spectrometer using KBr discs. [1]H and ^{31}P nuclear magnetic resonance (NMR) spectra were obtained by a Bruker AV400 NMR spectrometer, and DPPC and DCM were dissolved in DMSO-d_6.

The curing behaviors of EP mixtures (~10.0 mg) were studied by a Perkin-Elmer DSC 4000 under nitrogen atmosphere. The heating rate was 5, 10, 15 or 20 K/min. The rheological behaviors were investigated on a MCR302 (Anton Paar, Austria) at a constant frequency of 1 Hz and a heating rate of 5 °C/min, with the shear torque controlled below 150 mN·m.

Thermogravimetric analysis (TGA) was performed on a NETZSCH STA449F3 thermal gravimetric analyzer under a nitrogen flow of 20 mL/min, and a powdered sample (~7 mg) was tested at the heating rate of 10 °C/min. Dynamic mechanical analysis (DMA) was conducted in a three-point bending mode on a TA DMA Q800 instrument. The heating rate was 5 °C/min, the specimen dimension was 20 mm × 1 mm × 4 mm, and the constant frequency was 1.0 Hz. The tensile and flexural properties of EP thermosets were investigated using a LE5105 microcomputer-controlled electronic universal testing machine (LISHI Instrument, China) based on ASTM D3039 and D790 standards at the speed of 1 mm/min. The impact strength of EP samples (*size*: 80 mm × 10 mm × 4 mm) was investigated by a XJJD-50 impact tester (Jinjian Testing Instrument, China) according to GB/T 2667–2008 standard. The reported results were the averages of five specimens.

Limiting oxygen index (LOI) of EP samples (*size*: 100 mm × 6.5 mm × 3 mm) was recorded on a JF-3 oxygen index meter (Jiangning Analysis Instrument, China) according to ASTM D2863 standard. Vertical burning (UL-94) classification of EP samples (*size*: 130 mm × 13 mm × 3 mm) was measured by a NK8017A instrument (Nklsky Instrument, China) based on ASTM D3801 standard. Combustion behaviors of EP samples (*size*: 100 mm × 100 mm × 3 mm) were studied based on ISO 5660 standard by a FTT cone calorimeter (Fire Testing Technology, UK) under an external flux of 50 kW/m^2.

The gaseous decomposition products of EP samples were explored by a TGA coupled with a FTIR (TG-IR, Thermo-Nicolet iS-10) in nitrogen and air conditions, and the heating rate was 20 °C/min. Pyrolysis gas-chromatography-mass spectrometry (Py-GC/MS) analysis was applied to evaluate the pyrolysis process of DCM on a 5200 + pyrolyzer (CDS, U. S.) that was linked to a CLARUS SQ 8T system (PerkinElmer, U.S.). Powdered sample was about 5 mg, and the pyrolysis temperature was 500 °C.

The infrared thermal images of the burning samples were recorded by a TIX 1000 infrared thermal imager (FLUKE, Germany). The temperature distribution on the backside of the sample was recorded for 60 s when its frontside was subjected to flame impact. The microstructure and chemical component of fractured surface and residual char were investigated by a QuantaFEG450 scanning electron microscope (SEM, FEI, U.S.) coupled with an energy dispersive spectrometer (EDS) under an acceleration voltage of 15 kV. Raman spectrum of char residue was obtained by an Invia Raman microscope (Renishaw, UK) at 532 nm argon ion laser. X-ray photoelectron spectroscopy (XPS) was performed on a ESCALAB 250Xi X-ray photoelectron spectrometer (Thermo Fisher Scientific, U.S.) with a Al Ka radiation (1486.6 eV).

3. Results and discussion

3.1. Characterization of DCM

The chemical structure of DCM was characterized by ^{1}H NMR, ^{31}P NMR, and FTIR. The FTIR spectra of DMP-30 and DCM are presented in Fig. 1b. Both FTIR spectra showed the typical absorption peaks of –CH$_3$ group at 2942 and 1357 cm^{-1} [32]. The peaks located at 2813 and 2769 cm^{-1} were assigned to the stretching vibration of –CH$_2$- group [33,34]. The characteristic peaks at 1612 and 1456 cm^{-1} belonged to the phenyl [35,36]. The peak at 1257 cm^{-1} was assigned to the C-N bond [37]. The absorption peak at 1174 cm^{-1} was corresponded to the -O-Ph structure [38]. For DCM, the absorption band at 3054 cm^{-1} belonged to the -C-H of phenyl [39], and those at 903 and 1127 cm^{-1} belonged to the P-O-Ph and -P=O groups, respectively [40]. All these results confirmed that DCM was synthesized by the reaction of DMP-30 and DPPC.

As displayed in the ^{1}H NMR spectrum of DCM (see Fig. 1c), the chemical shifts at 7.11–7.94 ppm belonged to the protons (H$_a$, H$_b$, H$_c$ and H$_f$) of phenyl, those at 3.39–3.65 and 3.13 ppm were attributed to the protons (H$_e$ and H$_h$) of –CH$_3$ group, and those at 2.13–2.30 and 1.91 ppm were attributed to the protons (H$_d$ and H$_g$) of –CH$_2$- group. The integral area ratio of these three regions was about 6:9:2, which was closed to the theoretical proton number ratio (H$_{a+b+c+f}$: H$_{e+h}$: H$_{d+g}$), further demonstrating the successful synthesis of DCM. Furthermore, DPPC exhibited one peak at 24.1 ppm in the ^{31}P NMR spectrum, while DCM showed two peaks at 14.2 and 29.2 ppm (see Fig. 1d), which was probably because the isomers were existed in the structure of DCM. Similar result had also been reported in previous works on phosphorus-derived flame retardants [41,42]. The ^{1}H NMR, ^{31}P NMR, and FTIR results had determined that DCM was successfully synthesized.

3.2. Curing/rheological behaviors of EPs

Understanding curing reaction kinetics is essential for setting curing procedure and achieving desirable products [43]. The curing reaction kinetics of EP/DMP-30 and EP/DCM-1.5 was investigated by the non-isothermal DSC at the heating rates of 5, 10, 15, and 20 K/min, and the corresponding plots and parameters are shown in Fig. 2a-c and Table S1. The activation energy (E_a) and reaction rate equation of EP/DMP-30 and EP/DCM-1.5 were obtained by the Kissinger, Ozawa and Crane methods [44,45].

As presented in Fig. 2a, all EPs showed only one exothermic peak, and the peak temperatures of the DCM-containing EPs were about 26 °C high than that of EP/DMP-30, suggesting that the introduction of phosphorous-containing group reduced the curing activity of tertiary amine group in DMP-30. Meanwhile, the peak temperatures of EP/DMP-30 and EP/DCM-1.5 gradually increased with the increase of heating rate due to the hysteresis effect of curing reaction (see Fig. 2b, c) [8]. As presented in Table S1, although the peak temperature of EP/DMP-30 was lower than that of EP/DCM-1.5, the E_a of EP/DMP-30 (64.8 kJ/mol) was much higher than that of EP/DCM-1.5 (49.9 kJ/mol). Obviously, the curing temperature and E_a of these two systems are closely related to the system viscosity and tertiary amine content [46,47]. The viscosity of EP/DMP-30 was much lower than that of EP/DCM-1.5 due to the lower viscosity of DMP-30 than DCM and the lower amount of addition. Benefiting from its lower viscosity, EP/DMP-30 was able to cure at a lower temperature with the catalysis of tertiary amine groups. By contrast, EP/DCM-1.5 with higher viscosity needed a higher temperature to activate the curing reaction. Notably, the tertiary amine content of EP/DCM-1.5 was higher than that of EP/DMP-30, which led
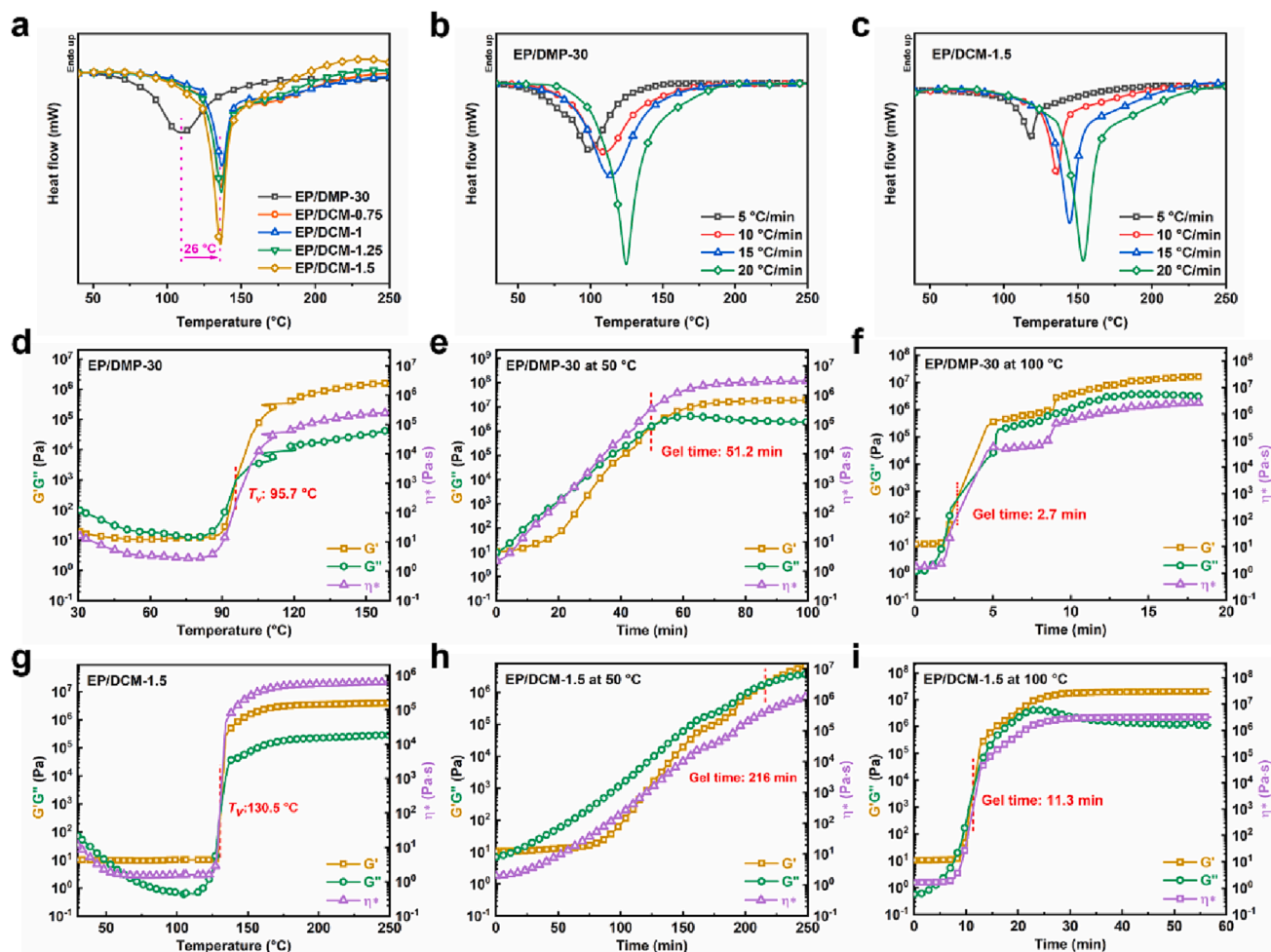
Fig. 2. (a) Non-isothermal DSC curves of EPs at the heating rate of 10 K/min; non-isothermal DSC curves of (b) EP/DMP-30 and (c) EP/DCM-1.5; (d) storage modulus (G'), loss modulus (G''), and complex viscosity (η*) curves of EP/DMP-30 as a function of temperature; G', G'' and η* curves of EP/DMP-30 at (e) 50 and (f) 100 °C; (g) G', G'' and η* curves of EP/DCM-1.5 as a function of temperature; and G', G'' and η* curves of EP/DCM-1.5 at (h) 50 and (i) 100 °C.

to the reduced E_a. In addition, the n values of EP/DMP-30 and EP/DCM-1.5 were 0.93 and 0.91, respectively, implying that the curing of both systems was a first-order reaction.

The rheological behaviors of EP/DMP-30 and EP/DCM-1.5 were also investigated, with the relevant curves presented in Fig. 2d-i. As the temperature increases, the temperature at which the G' and G'' curves intersect is defined as the gel point (T_v), indicating the transition from viscous to solid states [48,49]. At a certain temperature, the time at the intersection of the G' and G'' curves is defined as the gel time. As presented in Fig. 2d, g, the T_v of EP/DCM-1.5 was 34.8 °C higher than that of EP/DMP-30. Additionally, the gel time of EP/DCM-1.5 (216 and 11.3 min) was longer than that of EP/DMP-30 (51.2 and 2.7 min) at 50 and 100 °C, respectively (see Fig. 2e, f, h and i). Such results further demonstrated that the reactivity of DCM was lower than that of DMP-30 due to the steric-hindrance effect of P-containing group. Notably, at a low temperature, EP/DCM-1.5 exhibited a long processability time, while it can be cured rapidly at a modest temperature, indicative of superior processability.

3.3. Thermal properties of EPs

The DMA and TGA techniques were employed to investigate the thermal properties of EP/DMP-30 and EP/DCM samples, with the relevant plots shown in Fig. 3. Some important parameters, including glass transition temperature (T_g), storage modulus (E') at 50 °C, crosslinking

density (v_e), temperature at 5% mass loss ($T_{5\%}$), temperature at maximum mass loss rate (T_{max}), maximum weight loss rate (R_{max}), and char yield at 800 °C (*CY*) are listed in Table S2. The v_e of EP was calculated according to the classical theory of rubber elasticity [50]. As displayed in Fig. 3a and Table S2, the E' values of EP/DCM samples at 50 °C were higher than that of EP/DMP-30 sample, indicating that the stiffness of EP was increased with the incorporation of phosphorus-derived group. Nevertheless, the E' of EP/DCM-1.5 at 50 °C was slightly lower than that of EP/DCM-1.25 due to the reduced crosslinking density. Meanwhile, the T_g values of EP/DCM samples were closed to or even higher than that of EP/DMP-30 sample (see Fig. 3b and Table S2), demonstrating that the heat resistance of EP was not affected after covalently introducing phosphorus-derived group. Obviously, the introduction of P-containing group can enhance both heat resistance and mechanical stiffness of EP/DCM samples.

In Fig. 3c and d, all EP samples underwent one-step degradation in N_2 condition. The $T_{5\%}$ and T_{max} values of EP/DCM samples were lower than those of EP/DMP-30 sample, which gradually decreased with the increasing phosphorus content (see Table S2). The decreased $T_{5\%}$ and T_{max} signified that the phosphorus-containing degradation products of DCM catalyzed the decomposition of the EP matrix. Similar catalysis had also been reported in previous works on phosphorus-containing polymeric materials [51,52]. Notably, all EP/DCMs displayed lower R_{max} and higher *CY* values than EP/DMP-30 (see Table S2). For instance, the R_{max} value of EP/DCM-1.5 was decreased from 11.4 %/min of EP/DMP-
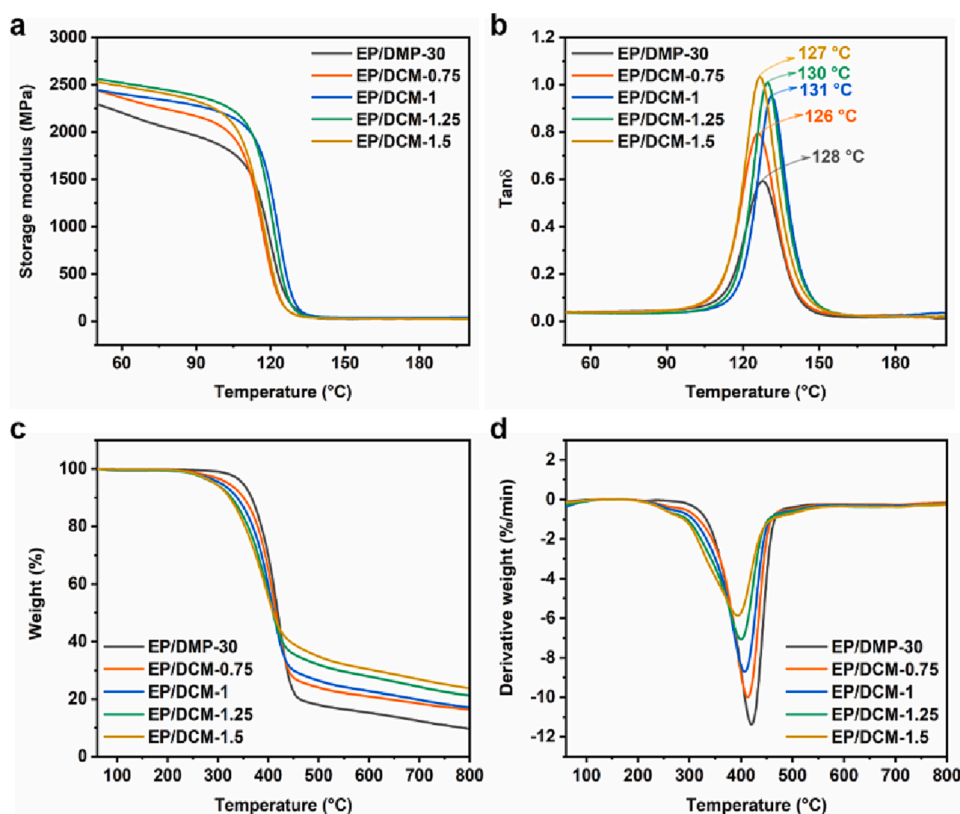
Fig. 3. (a) Storage modulus, (b) Tan delta, (c) TG, and (d) DTG curves of EPs under nitrogen atmosphere.

30 to 5.9 %/min, and the *CY* value was increased from 9.8% of EP/DMP-30 to 24.1%. Such results implied that the phosphorus-based decomposition products derived from DCM promoted the char formation, thus retarding the thermal decomposition of the matrix at high temperatures. In sum, EP/DCM samples exhibited superior heat resistance, char-forming capacity and mechanical stiffness to EP/DMP-30 sample due to the presence of P-containing group.

3.4. Mechanical properties of EPs

The mechanical properties of EP/DMP-30 and EP/DCM thermosets were explored, with the results shown in Fig. S1 and Table 2. The mechanical properties of the DCM-cured EP thermosets were significantly improved relative to those of EP/DMP-30 thermoset. For example, the tensile strength, tensile modulus, elongation at break, flexural strength, flexural modulus and impact strength of EP/DCM-1.25 were up to 79.8 MPa, 3243 MPa, 8.6%, 116.3 MPa, 3173 MPa and 20.3 kJ/m^2, which were 61.2%, 19.4%, 72.0%, 43.6%, 8.9% and 198.5% higher than those of EP/DMP-30, respectively. The improved mechanical stiffness, strength and toughness were mainly due to the increased crosslinking density and incorporation of rigid P-containing group. In addition, the tensile strength, flexural strength, elongation at break and impact strength of EP/DCM thermosets increased first and then decreased with the increasing DCM content, and both tensile and flexural moduli were almost positively correlated with the DCM content. Such results indicated that the incorporation of rigid P-containing groups was conducive to improving the rigidity of EP thermosets, but excessive DCM led to reduced crosslinking density and mechanical robustness and toughness.

The toughening mechanism of DCM was investigated by SEM technique, with the SEM images of the fractured surfaces for EPs after impact tests presented in Fig. 4a-c. Apparently, the cross-section of EP/DMP-30 was regular and smooth, showing typical brittle rupture characteristics. In contrast, the cross-sections of both EP/DCM-1 and EP/DCM-1.5 were rough, and numerous ripples and crinkles appeared. These ripples and crinkles absorbed part of the energy when the EP matrix was subjected to an external impact, thus leading to the energy dissipation, and enhancing the toughness. Moreover, no aggregation was observed within the cross-sections of EP/DCM-1 and EP/DCM-1.5, indicative of good compatibility between DCM and EP. With appropriate addition of DCM, the obtained EP thermoset exhibited superior mechanical stiffness, robustness and toughness.

Table 2
The mechanical properties of EP samples.

| Sample	Tensile strength (MPa)	Tensile modulus (MPa)	Elongation at break (%)	Flexural strength (MPa)	Flexural modulus (MPa)	Impact strength (kJ/m^2)
EP/DMP-30	49.5 ± 2.5	2717 ± 136	5.0 ± 0.2	81.0 ± 4.1	2915 ± 145	6.8 ± 0.3
EP/DCM-0.75	69.1 ± 3.5	2792 ± 139	7.7 ± 0.3	93.6 ± 4.7	3056 ± 152	18.8 ± 0.9
EP/DCM-1	74.5 ± 3.7	2996 ± 149	8.0 ± 0.4	93.1 ± 4.7	3196 ± 159	24.7 ± 1.2
EP/DCM-1.25	79.8 ± 4.0	3243 ± 162	8.6 ± 0.4	116.3 ± 5.8	3173 ± 158	20.3 ± 1.0
EP/DCM-1.5	77.1 ± 3.9	3276 ± 163	7.1 ± 0.3	112.5 ± 5.6	3410 ± 170	21.4 ± 1.1
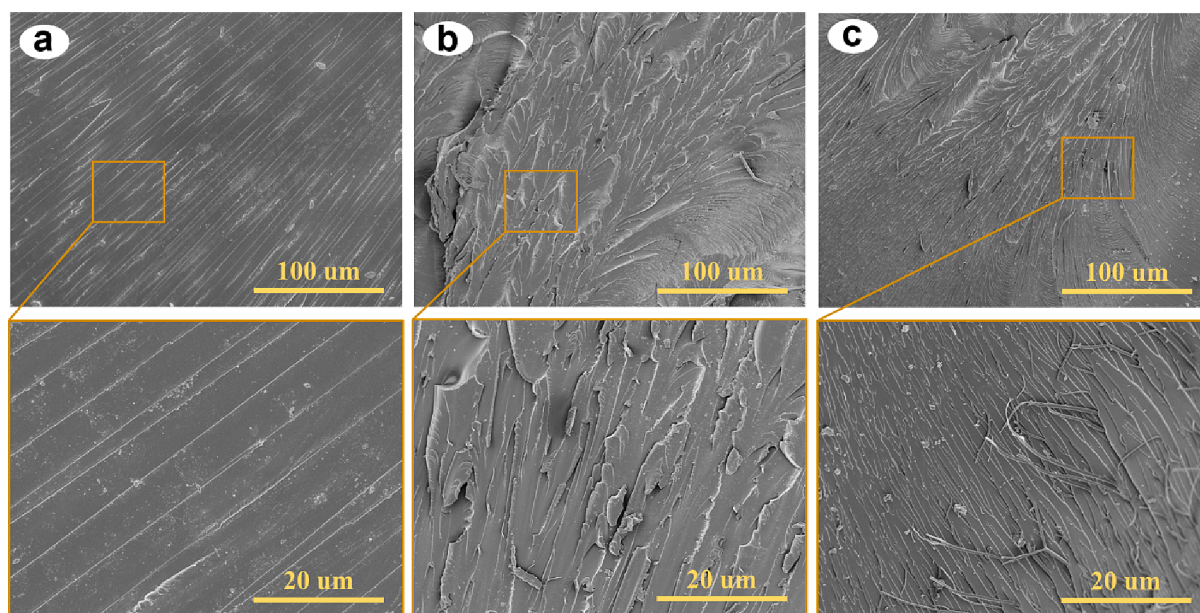
Fig. 4. SEM images of the fractured surfaces for (a) EP/DMP-30, (b) EP/DCM-1, and (c) EP/DCM-1.5 thermosets after impact tests.

3.5. Flame-retardant properties of EPs

Firstly, the LOI and UL-94 tests were applied to evaluate the flame retardancy of EP/DMP-30 and EP/DCM samples. As presented in Table S3, EP/DMP-30 was highly combustible, and its LOI value was 20.1%. During the UL-94 test, EP/DMP-30 couldn't self-extinguish and produced severe molten droplets, thus it was unable to pass any rating. In comparison, when the DCM-cured EPs were ignited, they all self-extinguished within 3 s, and the molten droplets disappeared. Therefore, all DCM-cured EPs reached a UL-94 V-0 classification. Meanwhile, all DCM-cured EPs presented higher LOI values than EP/DMP-30, and the LOI values gradually increased with increasing DCM contents. For instance, the LOI values of EP/DCM-1.0 and EP/DCM-1.5 increased to 34.1% and 35.7%, respectively. These results clearly demonstrated that DCM effectively improved the flame retardancy of EP thermosets.

The cone calorimeter is the most common experimental apparatus to characterize the combustion behaviors of polymeric materials [53–55]. The combustion characteristic curves and parameters of EP/DMP-30 and EP/DCM samples obtained from cone calorimetry tests are displayed in Fig. 5 and Table S4. As presented in Table S4, EP/DMP-30 released a large amount of heat and toxic smoke during burning, and its PHRR, THR, PSPR and TSP were as high as 1647 kW/m^2, 119.3 MJ/m^2, 0.31 m^2/s and 24.5 m^2, respectively. By contrast, the PHRR, THR, PSPR and TSP of all DCM-cured EPs decreased obviously due to the introduction of P-containing group. In particular, EP/DCM-1.5 with the highest phosphorus content exhibited the lowest heat release and smoke generation among all EPs, of which the PHRR, THR, PSPR and TSP displayed 36.2%, 37.0%, 22.6% and 14.3% reductions relative to those of EP/DMP-30. These results demonstrated that the phosphorus-derived group in DCM efficiently inhibited the heat and smoke release of the EP matrix, thus improving the flame retardancy and smoke suppression.
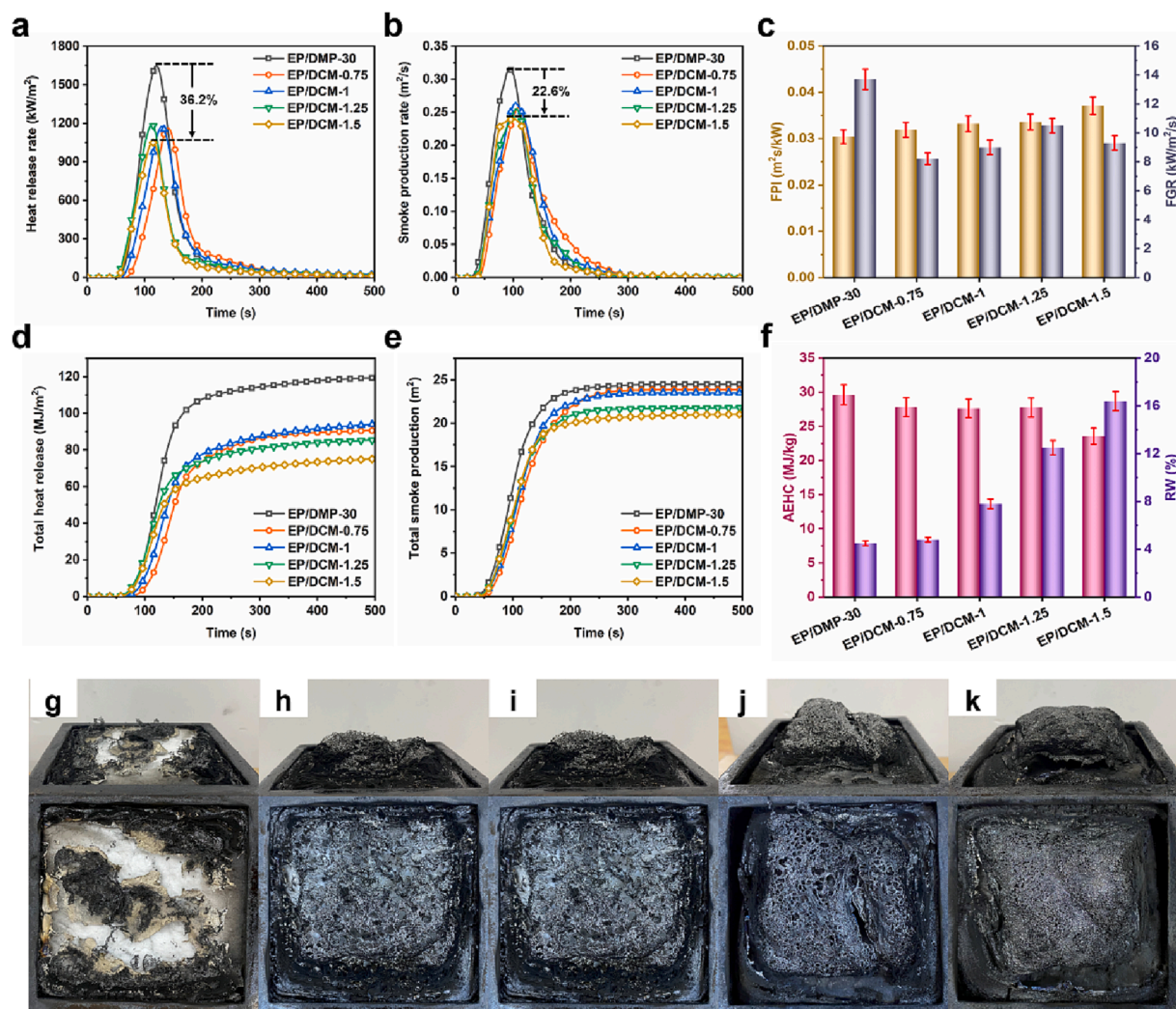
The fire performance index (FPI) and fire growth rate (FGR) are another two critical parameters to assess the fire safety of polymeric materials [13]. As exhibited in Fig. 5c and Table S4, the FPI values of the DCM-cured EPs were all higher than that of EP/DMP-30, indicative of the reduced fire hazard. Additionally, the FGR values of the DCM-cured EPs were all lower than that of EP/DMP-30, further demonstrating the enhanced fire safety. Obviously, the introduction of P-containing group was responsible for the enhanced fire safety of EP. The average effective heat of combustion (AEHC) is often applied to evaluate the burning degree of pyrolysis products in the gas phase [37,56]. In Fig. 5f and

Table S4, the AEHC values of the DCM-cured EPs were all lower than that of EP/DMP-30. For instance, the AEHC of EP/DCM-1.5 was reduced from 29.6 MJ/kg of EP/DMP-30 to 23.6 MJ/kg, by 20.3%. Such results verified that the P-containing group in DCM released the P-derived radicals (*e.g.,* HPO• and PO•) to eliminate the active radicals (*e.g.,* OH• and H•) derived from the matrix during burning, thus inhibiting the combustion reaction in the gas phase [57–59]. In Fig. 5f and Table S4, EP/DCM-1.5 showed the highest residual weight (RW) at 500 s among all EPs, which increased by 264.4% compared with that of EP/DMP-30, demonstrating that the P-based group in DCM also facilitated the carbonization of the matrix in the condensed phase. Moreover, the char of EP/DMP-30 was broken and fragile (see Fig. 5g), while those of EP/DCMs showed intumescent and compact structures (see Fig. 5h-k), which were conducive to inhibiting the exchange of heat and oxygen and release of smoke [60,61]. In sum, DCM was effective in enhancing the flame retardancy and smoke suppression of EP by the gas/condensed-phase flame-retardant functions of its phosphorus-containing group.

3.6. Flame-retardant mode-of-action

3.6.1. Gas-phase analysis

The decomposition gaseous products of EP/DMP-30 and EP/DCM-1.5 were studied by TG-FTIR technique in N_2 and air conditions, with the spectra displayed in Fig. 6 and S2. As shown in Fig. 6a, b, d, e, the decomposition gaseous products of EP/DMP-30 and EP/DCM-1.5 in air and nitrogen conditions were similar, but EP/DCM-1.5 exhibited lower intensities of the absorption peaks. As shown in Fig. 6c, f, the main gaseous products of EP/DMP-30 and EP/DCM-1.5 mainly included H_2O/phenol (3652 cm^{-1}), hydrocarbon compounds (3151–2769 cm^{-1}), CO_2 (2360 and 551 cm^{-1}), CO (2183 cm^{-1}), carbonyl compounds (1731 cm^{-1}), aromatic compounds (1604, 1508, 829 and 747 cm^{-1}), ether compounds (1253 and 1176 cm^{-1}), and NH_3 (929 cm^{-1}) [23,45]. Notably, the characteristic peak of P-O-C was detected at 1122 cm^{-1} in the FTIR spectra of gaseous products for EP/DCM-1.5 (see Fig. 6f, S2b), which further confirmed that the P-containing group in DCM can produce P-derived fragments in the gas phase under heating, which can further decompose to generate P-containing radicals with radical quenching effect. Hence, the gas-phase flame-retardant effect of DCM was mainly attributed to the radical quenching function of its P-containing group.

Fig. 5. The curves of (a) heat release rate (HRR) and (b) smoke production rate (SPR), the values of (c) fire performance index (FPI) and fire growth rate (FGR), the curves of (d) total heat release (THR) and (e) total smoke production (TSP), the values of (f) average effective heat of combustion (AEHC) and residual weight (RW) for EP thermosets, and digital photographs of (g) EP/DMP-30, (h) EP/DCM-0.75, (i) EP/DCM-1, (j) EP/DCM-1.25, and (k) EP/DCM-1.5 chars from top and side views.
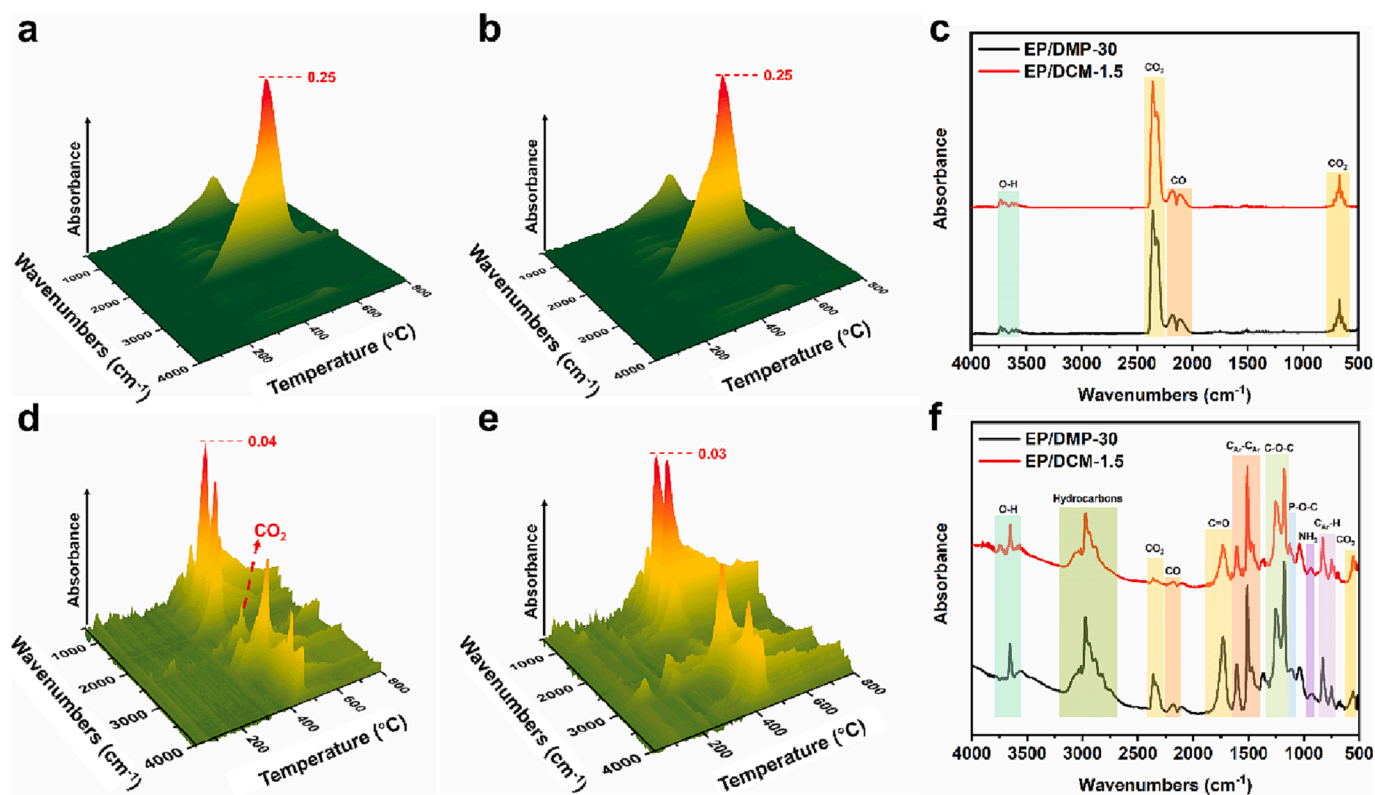
Fig. 6. 3D TG-FTIR spectra of gaseous decomposition products for (a, d) EP/DMP-30 and (b, e) EP/DCM-1.5 under air and N_2 atmosphere; and FTIR spectra of gaseous decomposition products for EP/DMP-30 and EP/DCM-1.5 at T_{max} under (c) air and (f) N_2 atmosphere.
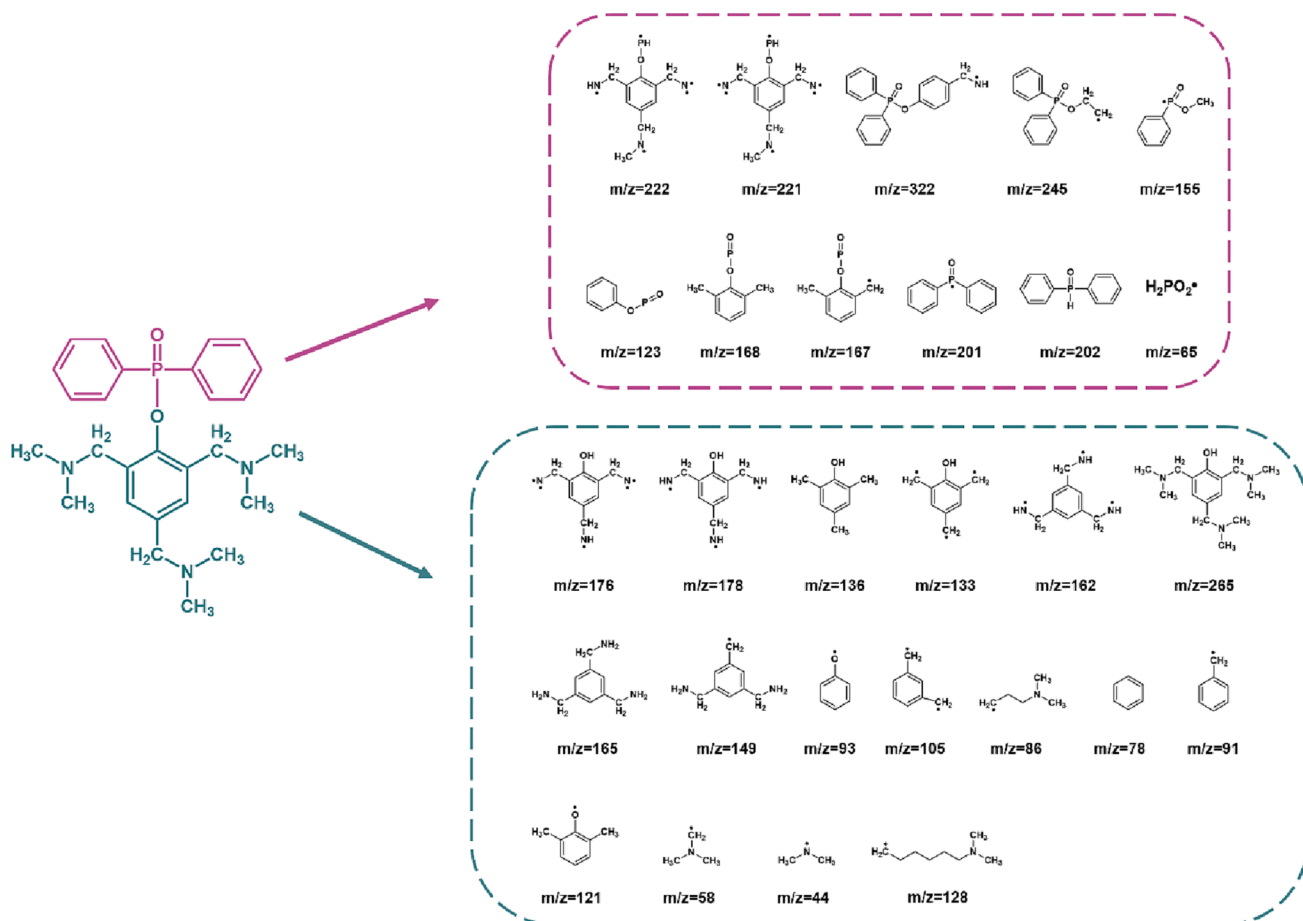

Fig. 7. Proposed pyrolysis route of DCM during the py-GC/MS test.

To further investigate the gas-phase mechanism, py-GC/MS was employed to explore the pyrolysis fragments of DCM under heating. The total ion chromatogram (TIC), mass spectra at different retention time, and proposed pyrolysis route of DCM are shown in Fig. S3, S4 and 7. In the initial pyrolysis stage of DCM, the nitrogen-containing fragments (*m/z*: 44, 58 and 86) and phenol derivatives (*m/z*: 93, 121, 133 and 136) were detected, which was mainly due to the breakage of C-N and C-O bonds. As the pyrolysis of DCM proceed, the phosphorus-containing fragments (*m/z*: 201, 202, 221, 222, 245 and 322) were released due to the further pyrolysis of DCM. Hence, DCM released the nitrogen-containing gases and phosphorus-derived fragments when heated, which were able to dilute the concentration of combustible volatiles and capture the active radicals, respectively. When the EP matrix burned, DCM decomposed to release nitrogen- and phosphorus-based fragments to suppress the burning reaction in the gas phase.

3.6.2. Condensed-phase analysis

To explore the condensed-phase mechanism, the infrared thermal imager was applied to record the real-time temperature on the backside of EP/DMP-30 and EP/DCM-1.5 impacted by high-temperature flame (see Fig. 8a), with the infrared graphs presented in Fig. 8b. Apparently, EP/DMP-30 was highly combustible, and it was easily ignited. When EP/DMP-30 was exposed to the flame for 25 s, it was completely burned through, and the maximum temperature (T_{MAX}) and average temperature (T_{AV}) on the backside rapidly increased to > 500 and 231.7 °C, respectively. In contrast, EP/DCM-1.5 quickly formed an intumescent and compact char layer on its frontside when attacked by flame, and thus the T_{MAX} and T_{AV} of its backside were only 179.6 and 150.1 °C, respectively, at 30 s. In addition, the formed char layer of EP/DCM-1.5 was still unbroken at 60 s, indicating its reliability. Obviously, the DCM-cured EPs can rapidly form an intumescent and compact char layer on its surface during burning because of the promoting carbonization function

of P-derived group.

To further elaborate the flame-retardant mechanism of DCM in the condensed phase, the char residues obtained from the cone calorimetry tests were collected and investigated by SEM, EDS, Raman and XPS, respectively. As shown in Fig. S5a, the residual char surface of EP/DMP-30 was loose and broken. On the contrary, the residual char surface of EP/DCM-1.5 was compact and continuous (see Fig. S5b). In addition, the EDS spectrum in Fig. 9a showed that the residual char of EP/DMP-30 contained abundant carbon and oxygen, while the phosphorus and nitrogen were detected in the residual char of EP/DCM-1.5 (see Fig. 9b), which verified that the formation of a dense and intumescent char layer was mainly due to the flame-retardant functions of the DCM-derived decomposition products in the condensed phase. Meanwhile, the Raman spectra of EP/DMP-30 and EP/DCM-1.5 residues are shown in Fig. 9c. The degree of graphitization can be quantitatively analyzed by calculating the area ratio of D to G peaks (I_D/I_G), and the lower the I_D/I_G, the higher the degree of graphitization [18,26]. The I_D/I_G value of EP/DMP-30 char was 2.77, while that of EP/DCM-1.5 reduced to 2.41. Hence, the graphitization degree of EP/DCM-1.5 char was higher than that of EP/DMP-30 char. Obviously, the highly graphitized char covered on the surface of the EP matrix, suppressing the heat transfer and smoke release, thus improving the flame retardancy and smoke suppression.

The XPS spectra of EP/DMP-30 and EP/DCM-1.5 residues are presented in Fig. 9d-i. Only carbon and oxygen were detected in the char of EP/DMP-30, while nitrogen and phosphorus appeared in the char of EP/DCM-1.5 in addition to C and O, which was consistent with the EDS results, further demonstrating the condensed-phase flame-retardant function of DCM. The high-resolution C1s and O1s spectra of EP/DMP-30 char are displayed in Fig. 9e and f, and the high-resolution C1s, O1s, and P2p spectra of EP/DCM-1.5 char are shown in Fig. 9g-i. In the C1s spectrum of EP/MP-30 residue (see Fig. 9e), the C-C/C=C, C-O, and C=O peaks were located at 284.4, 285.0, and 288.4 eV, respectively
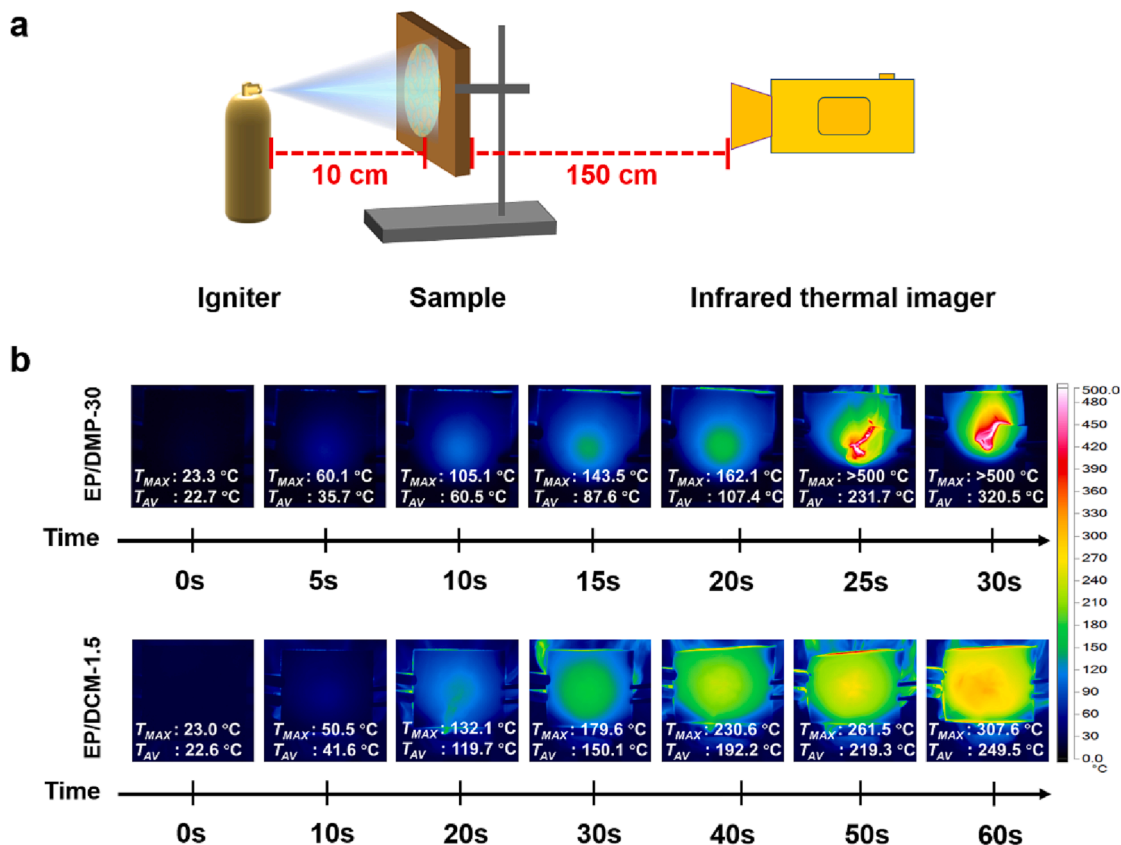

Fig. 8. (a) Illustration of flame impact test, and (b) thermal infrared images of the backside of EP/DMP-30 and EP/DCM-1.5.
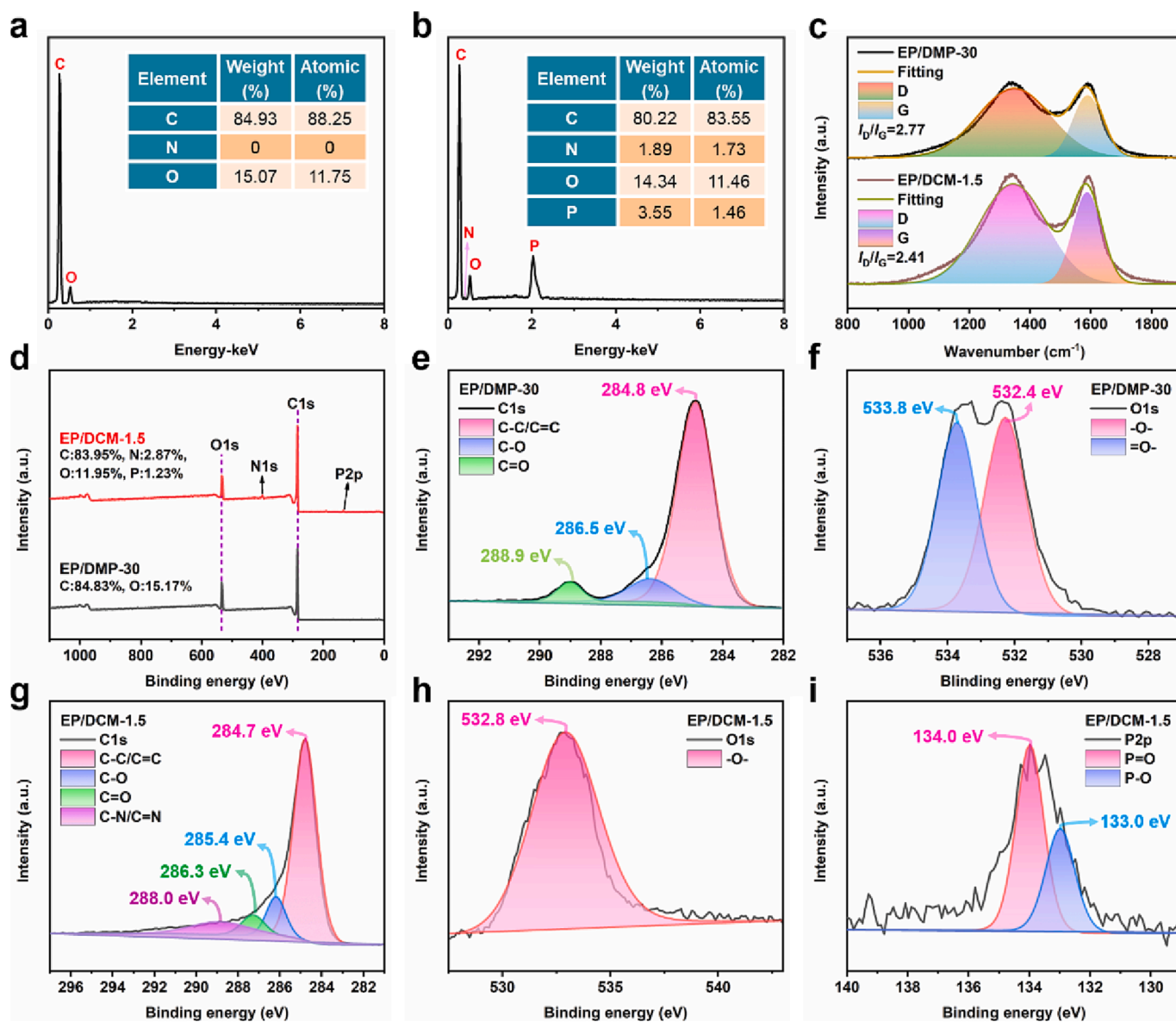
Fig. 9. EDS spectra of (a) EP/DMP-30 and (b) EP/DCM-1.5 chars; (c) Raman spectra of EP/DMP-30 and EP/DCM-1.5 chars; (d) XPS full-scan spectra and relative element contents of EP/DMP-30 and EP/DCM-1.5 chars; XPS high-resolution (e) C1s and (f) O1s spectra of EP/DMP-30 char; and XPS high-resolution (g) C1s, (h) O1s, and (i) P2p spectra of EP/DCM-1.5 char.

[25,56]. The peaks at 532.4 and 533.8 eV were attributed to -O- and =O in the O1s spectrum of EP/DMP-30 char (see Fig. 9f) [9,28]. However, the C1s spectrum of EP/DCM-1.5 char was divided into four peaks at 284.7, 285.4, 286.3, and 288.0 eV, which were assigned to C-C/C=C, C-O, C=O, and C-N/C=N, respectively (see Fig. 9g) [6,17]. The peak at 532.8 eV was assigned to -O- in the O1s spectrum of EP/DCM-1.5 char (see Fig. 9h) [4]. For the P2p spectrum of EP/DCM-1.5 char, the peaks at 133.0 and 144.0 eV belonged to P-O and P=O, respectively [13,21]. In sum, the P- and N-containing pyrolysis products of DCM functioned in the condensed phase, which facilitated the formation of a continuous and intumescent char layer on the matrix surface during burning, thereby suppressing the heat transfer and smoke generation.

Based on the above analyses, the potential flame-retardant mode-of-action of DCM is proposed in Fig. 10. In the gas phase, the phosphorus-containing radicals and nitrogen-based gases derived from DCM inhibited the burning reaction, thus reducing the burning degree. In the condensed phase, DCM decomposed to generate P- and N-containing pyrolysis products, which facilitated the EP matrix to form a compact

and intumescent char layer on its surface, which suppressed the heat release and smoke generation. Therefore, DCM exerted flame-retardant effects in both gaseous and condensed phases during combustion, thus significantly enhancing the flame retardancy and smoke suppression of EP thermoset.

4. Conclusions

In this work, a novel P-containing tertiary amine curing agent (DCM) was successfully synthesized *via* the elimination reaction of DMP-30 and DPPC. The comprehensive performances of the DCM-cured EPs were evaluated by various measurements. The DSC and rheological test results demonstrated that the introduction of P-containing group reduced the reactivity of tertiary amine groups in DCM and the EP/DCM systems featured good processability. Moreover, the EP/DCM thermosets showed superior heat resistance, charring capacity and mechanical properties to virgin EP/DMP-30 thermoset. Meanwhile, the DCM-cured EPs exhibited remarkable flame retardancy and smoke suppression. For
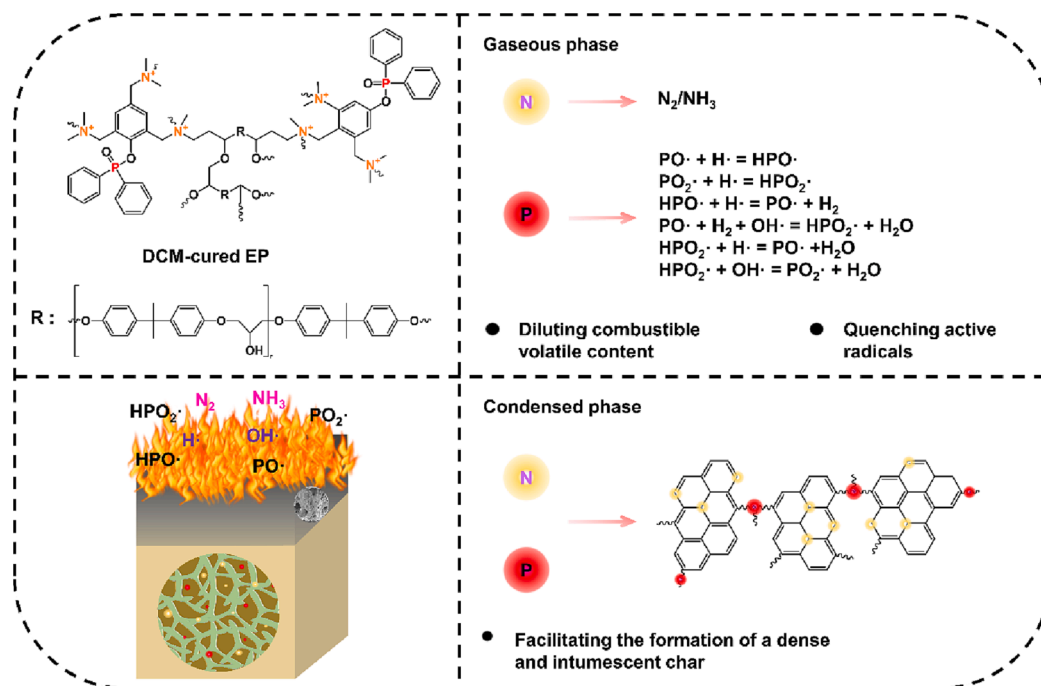
Fig. 10. Schematic diagram of flame-retardant mode-of-action of DCM.

instance, the LOI value and UL-94 rating of EP/DCM-1.5 sample reached 35.7% and V-0, respectively, and its PHRR, THR, TSP and PSPR were reduced by 36.2%, 37.0%, 14.3% and 22.6% relative to those of EP/DMP-30 sample. The significantly-enhanced fire safety of EP/DCMs was mainly due to the condensed/gas-phase flame-retardant effects of DCM. Hence, this work created a new generation of multifunctional flame-retardant curing agent for the fabrication of high-performance epoxy resins with superior heat resistance, mechanical properties, and fire safety.

Declaration of Competing Interest

The authors declare that they have no known competing financial interests or personal relationships that could have appeared to influence the work reported in this paper.

Data availability

The authors are unable or have chosen not to specify which data has been used.

Acknowledgement

Appendix A. Supplementary data

Supplementary data to this article can be found online at https://doi.org/10.1016/j.cej.2023.143811.

References

[1] X. Mi, N. Liang, H. Xu, J. Wu, Y. Jiang, B. Nie, D. Zhang, Toughness and its mechanisms in epoxy resins, Prog. Mater. Sci. 130 (2022), 100977, https://doi.org/10.1016/j.pmatsci.2022.100977.

[2] Y. Qi, Z. Weng, Y. Kou, J. Li, Q. Cao, J. Wang, S. Zhang, X. Jian, Facile synthesis of bio-based tetra-functional epoxy resin and its potential application as high-performance composite resin matrix, Compos. Part B Eng. 214 (2021), 108749, https://doi.org/10.1016/j.compositesb.2021.108749.

[3] Z. Chen, B. Yang, N. Song, T. Chen, Q. Zhang, C. Li, J. Jiang, T. Chen, Y. Yu, L. X. Liu, Machine learning-guided design of organic phosphorus-containing flame retardants to improve the limiting oxygen index of epoxy resins, Chem. Eng. J. 455 (2022), 140547, https://doi.org/10.1016/j.cej.2022.140547.

[4] Y. Tian, Q. Wang, L. Shen, Z. Cui, L. Kou, J. Cheng, J. Zhang, A renewable resveratrol-based epoxy resin with high Tg, excellent mechanical properties and low flammability, Chem. Eng. J. 383 (2020), 123124, https://doi.org/10.1016/j.cej.2019.123124.

[5] S. Yang, S. Huo, J. Wang, B. Zhang, J. Wang, S. Ran, Z. Fang, P. Song, H. Wang, A highly fire-safe and smoke-suppressive single-component epoxy resin with switchable curing temperature and rapid curing rate, Compos. Part B Eng. 207 (2021), 108601, https://doi.org/10.1016/j.compositesb.2020.108601.

[6] S. Huo, P. Song, B. Yu, S. Ran, V.S. Chevali, L. Liu, Z. Fang, H. Wang, Phosphorus-containing flame retardant epoxy thermosets: Recent advances and future perspectives, Prog. Polym. Sci. 114 (2021), 101366, https://doi.org/10.1016/j.progpolymsci.2021.101366.

[7] X. Wang, W. Guo, L. Song, Y. Hu, Intrinsically flame retardant bio-based epoxy thermosets: A review, Compos. Part B Eng. 179 (2019), 107487, https://doi.org/10.1016/j.compositesb.2019.107487.

[8] H. Nabipour, X. Wang, L. Song, Y. Hu, A high performance fully bio-based epoxy thermoset from a syringaldehyde-derived epoxy monomer cured by furan-derived amine, Green Chem. 23 (1) (2021) 501–510, https://doi.org/10.1039/d0gc03451g.

[9] J. Wang, X. Chen, J. Wang, S. Yang, K. Chen, L. Zhu, S. Huo, P. Song, H. Wang, High-performance, intrinsically fire-safe, single-component epoxy resins and carbon fiber reinforced epoxy composites based on two phosphorus-derived imidazoliums, Polym. Degrad. Stabil. 208 (2023), 110261, https://doi.org/10.1016/j.polymertesting.2020.106466.

[10] W. Rao, P. Zhao, C. Yu, H.-B. Zhao, Y.-Z. Wang, High strength, low flammability, and smoke suppression for epoxy thermoset enabled by a low-loading phosphorus-nitrogen-silicon compound, Compos. Part B Eng. 211 (2021), 108640, https://doi.org/10.1016/j.compositesb.2021.108640.

[11] M.A. Bhakare, K.D. Lokhande, M.P. Bondarde, P.S. Dhumal, S. Some, Dual functions of bioinspired, water-based, reusable composite as a highly efficient flame retardant and strong adhesive, Chem. Eng. J. 454 (2023), 140421, https://doi.org/10.1016/j.cej.2022.140421.

[12] Z. Chen, P. Xiao, J. Zhang, W. Tian, R. Jia, H. Nawaz, K. Jin, J. Zhang, A facile strategy to fabricate cellulose-based, flame-retardant, transparent and anti-dripping protective coatings, Chem. Eng. J. 379 (2020), 122270, https://doi.org/10.1016/j.cej.2019.122270.

[13] Q. Zhang, J. Wang, S. Yang, J. Cheng, G. Ding, S. Huo, Facile construction of one-component intrinsic flame-retardant epoxy resin system with fast curing ability using imidazole-blocked bismaleimide, Compos. Part B Eng. 177 (2019), 107380, https://doi.org/10.1016/j.compositesb.2019.107380.

[14] X.-F. Liu, B.-W. Liu, X. Luo, D.-M. Guo, H.-Y. Zhong, L. Chen, Y.-Z. Wang, A novel phosphorus-containing semi-aromatic polyester toward flame retardancy and enhanced mechanical properties of epoxy resin, Chem. Eng. J. 380 (2020), 122471, https://doi.org/10.1016/j.cej.2019.122471.

[15] Y.-F. Ai, L. Xia, F.-Q. Pang, Y.-L. Xu, H.-B. Zhao, R.-K. Jian, Mechanically strong and flame-retardant epoxy resins with anti-corrosion performance, Compos. Part B Eng. 193 (2020), 108019, https://doi.org/10.1016/j.compositesb.2020.108019.

[16] J. Cao, H. Duan, J. Zou, J. Zhang, C. Wan, C. Zhang, H. Ma, Bio-based phosphorus-containing benzoxazine towards high fire safety, heat resistance and mechanical properties of anhydride-cured epoxy resin, Polym. Degrad. Stabil. 198 (2022), 109878, https://doi.org/10.1016/j.polymdegradstab.2022.109878.

[17] Y. Han, H. Zhao, T. Gao, L. Chen, X. Wang, Y. Huang, L. Yuan, P. Zeng, Comparison of the performances of epoxy resin thermosets cured by two P-containing anhydrides, Polym. Degrad. Stabil. 200 (2022), 109937, https://doi.org/10.1016/j.polymdegradstab.2022.109937.

[18] H. Duan, Y. Chen, S. Ji, R. Hu, H. Ma, A novel phosphorus/nitrogen-containing polycarboxylic acid endowing epoxy resin with excellent flame retardance and mechanical properties, Chem. Eng. J. 375 (2019), 121916, https://doi.org/10.1016/j.cej.2019.121916.

[19] J. Li, Z. Weng, Q. Cao, Y. Qi, B. Lu, S. Zhang, J. Wang, X. Jian, Synthesis of an aromatic amine derived from biomass and its use as a feedstock for versatile epoxy thermoset, Chem. Eng. J. 433 (2022), 134512, https://doi.org/10.1016/j.cej.2022.134512.

[20] J. Peng, S. Xie, T. Liu, D. Wang, R. Ou, C. Guo, Q. Wang, Z. Liu, High-performance epoxy vitrimer with superior self-healing, shape-memory, flame retardancy, and antibacterial properties based on multifunctional curing agent, Compos. Part B Eng. 242 (2022), 110109, https://doi.org/10.1016/j.compositesb.2022.110109.

[21] Y.-F. Ai, F.-Q. Pang, Y.-L. Xu, R.-K. Jian, Multifunctional phosphorus-containing triazolyl amine toward self-intumescent flame-retardant and mechanically strong epoxy resin with high transparency, Ind. Eng. Chem. Res. 59 (26) (2020) 11918–11929, https://doi.org/10.1021/acs.iecr.0c01277.

[22] S. Huo, S. Yang, J. Wang, J. Cheng, Q. Zhang, Y. Hu, G. Ding, Q. Zhang, P. Song, A liquid phosphorus-containing imidazole derivative as flame-retardant curing agent for epoxy resin with enhanced thermal latency, mechanical, and flame-retardant performances, J. Hazard. Mater. 386 (2020), 121984, https://doi.org/10.1016/j.jhazmat.2019.121984.

[23] P. Gnanasekar, H. Chen, N. Tratnik, M. Feng, N. Yan, Enhancing performance of phosphorus containing vanillin-based epoxy resins by P-N non-covalently functionalized graphene oxide nanofillers, Compos. Part B Eng. 207 (2021), 108585, https://doi.org/10.1016/j.compositesb.2020.108585.

[24] F.-Q. Zhang, Y.-Z. Zhao, Y.-J. Xu, Y. Liu, P. Zhu, Flame retardation of vinyl ester resins and their glass fiber reinforced composites via liquid DOPO-containing 1-vinylimidazole salts, Compos. Part B Eng. 234 (2022), 109697, https://doi.org/10.1016/j.compositesb.2022.109697.

[25] J.-L. Huang, H.-L. Ding, X. Wang, L. Song, Y. Hu, Cardanol-derived anhydride cross-linked epoxy thermosets with intrinsic anti-flammability, toughness and shape memory effect, Chem. Eng. J. 450 (2022), 137906, https://doi.org/10.1016/j.cej.2022.137906.

[26] S. Huo, S. Yang, J. Wang, J. Cheng, Q. Zhang, Y. Hu, G. Ding, Q. Zhang, P. Song, H. Wang, A Liquid Phosphaphenanthrene-Derived Imidazole for Improved Flame Retardancy and Smoke Suppression of Epoxy Resin, ACS Appl. Polym. Mater. 2 (8) (2020) 3566–3575, https://doi.org/10.1021/acsapm.0c00577.

[27] J. Cheng, J. Wang, S. Yang, Q. Zhang, S. Huo, Q. Zhang, Y. Hu, G. Ding, Benzimidazolyl-substituted cyclotriphosphazene derivative as latent flame-retardant curing agent for one-component epoxy resin system with excellent comprehensive performance, Compos. Part B Eng. 177 (2019), 107440, https://doi.org/10.1016/j.compositesb.2019.107440.

[28] Q. Zhang, S. Yang, J. Wang, J. Cheng, Q. Zhang, G. Ding, Y. Hu, S. Huo, A DOPO based reactive flame retardant constructed by multiple heteroaromatic groups and its application on epoxy resin: curing behavior, thermal degradation and flame retardancy, Polym. Degrad. Stabil. 167 (2019) 10–20, https://doi.org/10.1016/j.polymdegradstab.2019.06.020.

[29] Q. Lian, H. Chen, Y. Luo, Y. Li, J. Cheng, Y. Liu, Toughening mechanism based on the physical entanglement of branched epoxy resin in the non-phase-separated inhomogeneous crosslinking network: An experimental and molecular dynamics simulation study, Polymer 247 (2022), 124754, https://doi.org/10.1016/j.polymer.2022.124754.

[30] H. Zhao, H. Duan, J. Zhang, L. Chen, C. Wan, C. Zhang, C. Liu, H. Ma, An Itaconic Acid-Based Phosphorus-Containing Oligomer Endowing Epoxy Resins with Good Flame Retardancy and Toughness, Macromol. Mater. Eng. 308 (2022) 2200550, https://doi.org/10.1002/mame.202200550.

[31] B. Chen, F. Wang, J.-Y. Li, J.-L. Zhang, Y. Zhang, H.-C. Zhao, Synthesis of Eugenol Bio-based Reactive Epoxy Diluent and Study on the Curing Kinetics and Properties of the Epoxy Resin System, Chinese J. Polym. Sci. 37 (5) (2019) 500–508, https://doi.org/10.1007/s10118-019-2210-7.

[32] J. Hayat, M. Akodad, A. Moumen, M. Baghour, A. Skalli, S. Ezrari, S. Belmalha, Phytochemical screening, polyphenols, flavonoids and tannin content, antioxidant activities and FTIR characterization of Marrubium vulgare L. from 2 different localities of Northeast of Morocco, Heliyon 6 (11) (2020), e05609, https://doi.org/10.1016/j.heliyon.2020.e05609.

[33] Z.-B. Shao, M.-X. Zhang, Y. Li, Y. Han, L. Ren, C. Deng, A novel multi-functional polymeric curing agent: Synthesis, characterization, and its epoxy resin with simultaneous excellent flame retardance and transparency, Chem. Eng. J. 345 (2018) 471–482, https://doi.org/10.1016/j.cej.2018.03.142.

[34] C. Wang, S. Huo, G. Ye, P. Song, H. Wang, Z. Liu, A P/Si-containing polyethylenimine curing agent towards transparent, durable fire-safe, mechanically-robust and tough epoxy resins, Chem. Eng. J. 451 (2023), 138768, https://doi.org/10.1016/j.cej.2022.138768.

[35] G. Ye, S. Huo, C. Wang, Q. Shi, L. Yu, Z. Liu, Z. Fang, H. Wang, A novel hyperbranched phosphorus-boron polymer for transparent, flame-retardant, smoke-suppressive, robust yet tough epoxy resins, Compos. Part B Eng. 227 (2021), 109395, https://doi.org/10.1016/j.compositesb.2021.109395.

[36] B. Hu, J. Wang, J. Wang, S. Yang, C. Li, F. Wang, S. Huo, P. Song, Z. Fang, H. Wang, Flame-retardant single-component epoxy resin cured by benzimidazolyl-substituted cyclotriphosphazene: storage stability, curing behaviors and flame retardancy, Polym. Degrad. Stabil. 204 (2022), 110092, https://doi.org/10.1016/j.polymdegradstab.2022.110092.

[37] J. Wang, S. Huo, J. Wang, S. Yang, K. Chen, C. Li, D. Fang, Z. Fang, P. Song, H. Wang, Green and Facile Synthesis of Bio-Based, Flame-Retardant, Latent Imidazole Curing Agent for Single-Component Epoxy Resin, ACS Appl. Polym. Mater. 4 (5) (2022) 3564–3574, https://doi.org/10.1021/acsapm.2c00138.

[38] L. He, T. Chen, Y. Zhang, L. Hu, T. Wang, R. Han, J.-L. He, W. Luo, Z.-G. Liu, J.-N. Deng, M.-J. Chen, Imide-DOPO derivative endows epoxy resin with excellent flame retardancy and fluorescence without losing glass transition temperature, Compos. Part B Eng. 230 (2022), 109553, https://doi.org/10.1016/j.compositesb.2021.109553.

[39] S. Seshadri, S. Gunasekaran, S. Muthu, Vibrational spectroscopy investigation using density functional theory on 7-chloro-3-methyl-2H-1,2,4- benzothiadiazine 1,1-dioxide, J. Raman Spectrosc. 40 (6) (2009) 639–644, https://doi.org/10.1002/jrs.2176.

[40] S. Huo, T. Sai, S. Ran, Z. Guo, Z. Fang, P. Song, H. Wang, A hyperbranched P/N/B-containing oligomer as multifunctional flame retardant for epoxy resins, Compos. Part B Eng. 234 (2022), 109701, https://doi.org/10.1016/j.compositesb.2022.109701.

[41] I. Oganesyan, J. Hajduk, J.A. Harrison, A. Marchand, M.F. Czar, R. Zenobi, Exploring Gas-Phase MS Methodologies for Structural Elucidation of Branched N-Glycan Isomers, Anal. Chem. 94 (29) (2022) 10531–10539, https://doi.org/10.1021/acs.analchem.2c02019.

[42] Y. Niihori, Y. Koyama, S. Watanabe, S. Hashimoto, S. Hossain, L.V. Nair, B. Kumar, W. Kurashige, Y. Negishi, Atomic and Isomeric Separation of Thiolate-Protected Alloy Clusters, J. Phys. Chem. Lett. 9 (17) (2018) 4930–4934, https://doi.org/10.1021/acs.jpclett.8b02211.

[43] S. Duan, H. Wu, K. Zhang, H. Liao, Z. Ma, F. Cheng, Effect of curing temperature on the reaction kinetics of cementitious steel slag-fly ash-desulfurized gypsum composites system, J. Build. Eng. 62 (2022), 105368, https://doi.org/10.1016/j.jobe.2022.105368.

[44] H. Wang, J. Yuan, Z. Zhu, X. Yin, Y. Weng, Z. Wang, F. Yang, J. Zhan, H. Wang, L. Wang, High performance epoxy resin composites modified with multifunctional thiophene/phosphaphenanthrene-based flame retardant: Excellent flame retardance, strong mechanical property and high transparency, Compos. Part B Eng. 227 (2021), 109392, https://doi.org/10.1016/j.compositesb.2021.109392.

[45] S. Tiwari, C.L. Gehlot, K. Srivastava, D. Srivastava, Simulation of the thermal degradation and curing kinetics of fly ash reinforced diglycidyl ether bisphenol A composite, J. Indian Chem. Soc. 98 (6) (2021), 100077, https://doi.org/10.1016/j.jics.2021.100077.

[46] M. Hesabi, A. Salimi, M.H. Beheshty, Effect of tertiary amine accelerators with different substituents on curing kinetics and reactivity of epoxy/dicyandiamide system, Polym. Test. 59 (2017) 344–354, https://doi.org/10.1016/j.polymertesting.2017.02.023.

[47] W. Zhao, L. An, S. Wang, Recyclable High-Performance Epoxy-Anhydride Resins with DMP-30 as the Catalyst of Transesterification Reactions, Polymers 13 (2) (2021) 296, https://doi.org/10.3390/polym13020296.

[48] M.R. Martínez-Miranda, V. García-Martínez, M.R. Gude, Gel point determination of a thermoset prepreg by means of rheology, Polym. Test. 78 (2019), 105950, https://doi.org/10.1016/j.polymertesting.2019.105950.

[49] L.C. Sow, S.J. Tan, H. Yang, Rheological properties and structure modification in liquid and gel of tilapia skin gelatin by the addition of low acyl gellan, Food Hydrocoll. 90 (2019) 9–18, https://doi.org/10.1016/j.foodhyd.2018.12.006.

[50] T. Ma, J. Ma, J. Zhang, J. Cheng, C. Yang, Curing behaviors and properties of epoxy resins with para-hexatomic ring blocks: Excellent comprehensive performances of tetrafluorophenyl, Polymer 206 (2020), 122828, https://doi.org/10.1016/j.polymer.2020.122828.

[51] Q. Shi, S. Huo, C. Wang, G. Ye, L. Yu, Z. Fang, H. Wang, Z. Liu, A phosphorus/silicon-based, hyperbranched polymer for high-performance, fire-safe, transparent epoxy resins, Polym. Degrad. Stabil. 203 (2022), 110065, https://doi.org/10.1016/j.polymdegradstab.2022.110065.

[52] J. Feng, Z. Ma, Z. Xu, H. Xie, Y. Lu, C. Maluk, P. Song, S. Bourbigot, H. Wang, A Si-containing polyphosphoramide via green chemistry for fire-retardant polylactide with well-preserved mechanical and transparent properties, Chem. Eng. J. 431 (2022), 134259, https://doi.org/10.1016/j.cej.2021.134259.

[53] T. Sai, S. Ran, S. Huo, Z. Guo, P. Song, Z. Fang, Sulfonated block ionomers enable transparent, fire-resistant, tough yet strong polycarbonate, Chem. Eng. J. 433 (2022), 133264, https://doi.org/10.1016/j.cej.2021.133264.

[54] Y. Qiu, L. Qian, Y. Chen, J. Hao, Improving the fracture toughness and flame retardant properties of epoxy thermosets by phosphaphenanthrene/siloxane cluster-like molecules with multiple reactive groups, Compos. Part B Eng. 178 (2019), 107481, https://doi.org/10.1016/j.compositesb.2019.107481.

[55] J. Zhang, X. Mi, S. Chen, Z. Xu, D. Zhang, M. Miao, J. Wang, A bio-based hyperbranched flame retardant for epoxy resins, Chem. Eng. J. 381 (2020), 122719, https://doi.org/10.1016/j.cej.2019.122719.

[56] Y.-Q. Shi, T. Fu, Y.-J. Xu, D.-F. Li, X.-L. Wang, Y.-Z. Wang, Novel phosphorus-containing halogen-free ionic liquid toward fire safety epoxy resin with well-

balanced comprehensive performance, Chem. Eng. J. 354 (2018) 208–219, https://doi.org/10.1016/j.cej.2018.08.023.

[57] X. Mu, Z. Jin, F. Chu, W. Cai, Y. Zhu, B. Yu, L. Song, Y. Hu, High-performance flame-retardant polycarbonate composites: Mechanisms investigation and fire-safety evaluation systems establishment, Compos. Part B Eng. 238 (2022), 109873, https://doi.org/10.1016/j.compositesb.2022.109873.

[58] L. Liu, M. Zhu, Z. Ma, X. Xu, S. Mohesen Seraji, B. Yu, Z. Sun, H. Wang, P. Song, A reactive copper-organophosphate-MXene heterostructure enabled antibacterial, self-extinguishing and mechanically robust polymer nanocomposites, Chem. Eng. J. 430 (2022), 132712, https://doi.org/10.1016/j.cej.2021.132712.

[59] Q. Zhang, J. Wang, S. Yang, J. Cheng, G. Ding, Y. Hu, S. Huo, Synthesis of a P/N/S-based flame retardant and its flame retardant effect on epoxy resin, Fire Safety J. 113 (2020), 102994, https://doi.org/10.1016/j.firesaf.2020.102994.

[60] X.-H. Shi, X.-L. Li, Y.-M. Li, Z. Li, D.-Y. Wang, Flame-retardant strategy and mechanism of fiber reinforced polymeric composite: A review, Compos. Part B Eng. 233 (2022), 109663, https://doi.org/10.1016/j.compositesb.2022.109663.

[61] J. Cheng, H. Duan, S. Yang, J. Wang, Q. Zhang, G. Ding, Y. Hu, S. Huo, A P/N-containing flame retardant constructed by phosphaphenanthrene, phosphonate, and triazole and its flame retardant mechanism in reducing fire hazards of epoxy resin, J. Appl. Polym. Sci. 137 (37) (2020) 49090, https://doi.org/10.1002/app.49090.